RSC Advances

ROYAL SOCIETY OF CHEMISTRY

www.rsc.org/advances

RSC Advances

ARTICLE

Bio-compatible Poly (ester-urethane) s based on PEG-PCL-PLLA Copolymer with Tunable Crystallization and Bio-degradation Properties

Received 00th January 20xx,
Accepted 00th January 20xx

DOI: 10.1039/x0xx00000x

www.rsc.org/

Guangzhong Yin[a,d], Donglin Zhao[a,b,d], Xiao Wang[c], Ye Ren[a,d], Lianwei Zhang[a,d], Xingxin Wu[c], Shaoping Nie[c], Qifang Li[a,b,d,*]

Multi-block copolymer poly (ester-urethane) s with ethoxy or polyhedral oligomeric silsesquioxanes (POSS) terminal functional groups were designed and synthesized by polyethylene glycol-poly(ε-caprolactone)-poly(L-lactide) (PEG-PCL-PLLA) diols via urethane linkages. In addition, an efficient and green catalyst, Bismuth ethylhexanoate, was used to prepare high molecular weight copolymers, and the influences of molecular compositions on the crystallinity, mechanical properties, biodegradability, cytocompatibility and blood-compatibility were systematically studied. By varying the terminal functional groups, as well as PEG, PCL and PLLA segment ratios, the materials exhibited highly tunable properties, especially including crystallinity, mechanical properties and degradation rate. Notably, these new functional materials may effectively be applied in the treatment of blood vessels because of the mentioned tunable properties.

Introduction

Poly(ε-caprolactone) (PCL) and poly(L-lactide) (PLLA) presented practical significance and great research value [1,2], and had been used widely as biodegradable polymer scaffolds for implantation of the human tissues, e.g. vascularized tracheal substitute [3], bone formation [4, 5] and cartilage regeneration matrix [6], and so on. An ideal tissue engineering materials should be able to mimic the structure of the native extracellular matrix, so as to provide mechanical support and regulate cellular activities. Generally, pure PCL or PLLA can't meet the functional requirements well. To address these limitations, several works have been performed to modify the functionality of polymer matrix. Some chemical methods were reported recently, for examples, Melchiorri et al. reported surface modification of PCL scaffold using Heparin [7], and Huang et al. prepared P (LLA-CL) copolymer to be an artificial blood vessel [8]. Numerous studies were mainly focused on technical level, modification via blending by electrospinning technique [9-13], surface modification of electrospun membranes [14, 15] or other technics [16, 17]. For examples, Kim et al. [16] prepared PCL/Alginate composite scaffolds multilayered 3D structure, which have potential for use in scaffolds for hard tissue regeneration. Zhang et al. [17] successfully accomplished PCL scaffolds by solvent casting/salt leaching and thermal induced phase separation (TIPS) methods, and genipin-cross-linked gelatin entrapped with recombinant human BMP-2 was exploited to decorate the interior surface of the scaffolds.

Biomaterials with tunable mechanics and controllable degradation rates should be taken into an important consideration when designing tissue engineering materials, because the degradation rate should ideally match the regeneration rate of cells and tissues [18, 19]. As well known, PCL presented slow degradation rate [20] and excellent flexibility; the PLLA was brittle materials, but with a faster degradation rate [21] In principle, control over mechanical properties and degradation rate can be sought through the preparation of novel copolymers covering a range of compositions. Indeed, the PCL-PLLA-based copolymers or the corresponding poly (ester-urethane) s were recently reported [22], especially, Peponi et al. [23, 24] synthesized tremendous related polymers varying both the molecular weight of the PCL and PLLA blocks as well as the relative content of each block in the copolymer, focusing on the relationship between their chemical compositions and their tailored final properties.

Polyethylene glycol (PEG) was widely used to improve the bio-compatibility of the blood contacting materials [25]. In addition, polyhedral oligomeric silsesquioxanes (POSS), a class of hybrid molecules with an inorganic silicon oxygen cage [26-28], which can generally improve thermal stability and mechanical properties, had good biocompatibility [29]. Mather et al. [30-32] reported the existence of POSS can effectively regulate the degradation of the material properties, because it can effectively regulate water absorption [33]. To achieve the performance requirements, PEG, PCL, PLLA and POSS were incorporated together in molecular level, resulting in linear

[a] State Key Laboratory of Chemical Resource Engineering, Beijing University of Chemical Technology, Beijing 100029, China
[b] Key Laboratory of Carbon fiber and functional polymers, Ministry of Education, Beijing University of Chemical Technology, Beijing 100029, China
[c] Emergency & Critical Care Center, Beijing Anzhen Hospital, Capital Medical University, Beijing, 100029, China
[d] College of Material Science and Engineering, Beijing University of Chemical Technology, Beijing 100029, China

PEG-PCL-PLLA-based tissue engineering materials. It was expected that the materials would exhibit highly tunable properties, including crystallinity, mechanical properties, controllable degradation rate and bio-compatibility. Notably, the current work is expected to provide valuable information for the development of new functional materials, which may effectively be applied in the treatment of blood vessels.

Experimental

Materials

ε-caprolactone (**ε**-CL, Alfa Aesar) was purified by vacuum distillation over Calcium hydride (CaH_2). PEG 2000 (Alfa Aesar) was dried in vacuum oven for 48 h at 95 °C. Dichloromethane (DCM) and toluene were purified by distillation over CaH_2 (Alfa Aesar). Stannous, 96% (Alfa Aesar), 1, 8-Diazabicyclo-[5.4.0]-undec-7-ene (DBU), 99% (J&K), L-(-)-Lactide, 99% (J&K), Hexa Methylenediisocyanate (HDI), 99% (J&K), Bismuth ethylhexanoate, 99% (J&K) and Aminopropyllsobutyl POSS, 99%, (Hybrid plastic) were used as received. Other solvents were obtained from Beijing Chemical works and used without any treatment.

The synthesis of PEG-PCL. The PEG-PCL polymer was synthesized by the ring-opening polymerization (ROP) of ε-caprolactone (ε-CL) using PEG as the initiator and stannous as the catalyst according to previous reports [34, 35]. Typically, PEG 2000 and ε-CL were weighed into Eggplant-type reaction flask. Then 0.2~0.5 wt. % of stannous was dropped into the mixture. The flask was immersed in an oil bath at 110 °C with magnetic stirring for 24 h under nitrogen purge. The product was dissolved in 20 mL $CHCl_3$, and precipitated into n-hexane (400 mL). After filtration and drying at vacuum oven at 40 °C for 24 h, a white product was obtained (>95% yield, Mn~15000 g/mol or 9800 g/mol by GPC). FTIR (cm^{-1}, KBr window): 3439 (-OH), 2946-2867 ($-CH_2-CH_2-$), 1726 (C=O), 1189 (C-O-C). ^1H NMR in $CDCl_3$ (ppm): δ4.245 (t, J=4.85Hz, $-OCH_2CH_2O(C=O)-$), δ4.081 (t, J=6.70Hz, $-CH_2CH_2O(C=O)-$), δ3.665 (s, $-OCH_2CH_2-$), δ2.327 (t, J=7.52Hz, $-O(C=O)-CH_2CH_2-$), δ1.711-1.628 (m, $-O(C=O)-CH_2CH_2-$), 1.441-1.365(m, $-CH_2CH_2CH_2-$).

The synthesis of PEG-PCL-PLLA. The PEG-PCL-PLLA was prepared according to previous reports [36]. Briefly, (i) PEG-PCL was dissolved in CH_2Cl_2 together with a predetermined amount of L-(-)-lactide in an oven-dried round-bottomed flask containing a magnetic stir bar. (ii) DBU was added at a concentration of 10 μL/mL. The solution was vigorously stirred under nitrogen purge. After 1.5 h, solid benzoic acid was added. As above, the PEG-PCL-PLLA was purified by precipitation twice into n-hexane from CH_2Cl_2 and dried at 50 °C under vacuum overnight. ^1H NMR in $CDCl_3$ (ppm): δ5.252 (q, J=7.05 Hz, $-O-(CH_3)CH-CO-$), δ4.247 (t, J=4.86Hz, $-OCH_2CH_2O(C=O)-$), δ4.083 (t, J=6.68Hz, $-CH_2CH_2O(C=O)-$), δ3.668 (s, $-OCH_2CH_2-$), δ2.329 (t, J=7.51Hz, $-O(C=O)-CH_2CH_2-$), δ1.712-1.629 (m, $-O(C=O)-CH_2CH_2-$, $-CO-C(CH_3)H-O-$), δ1.442-1.364 (m, $-CH_2CH_2CH_2-$).

Chain Extention. In a 100 mL of three necked flask, PEG-PCL-PLLA diols (10 g) were dissolved in toluene (50 mL), which had been dried with the aid of CaH_2. Under the protection of a nitrogen purge, the flask was heated to 95 °C, and a 0.5 mL of HDI was added to the 20 wt. % toluene solution. Several drops of Bismuth ethylhexanoate catalyst were added through a syringe. The reaction was kept at 95 °C for 12 h under the nitrogen purge, and a distinct viscosity rise was observed. After the full reaction, we added an appropriate amount of HDI to make sure we obtained NCO-terminated products. The polymer solution was then precipitated into an excess of anhydrous n-hexane and ether (V/V=1:1). FTIR (cm^{-1}, KBr window): 2946.07-2867.24 ($-CH_2-CH_2-$), 2230 (-NCO), 1726 (C=O), 1628-1530 (-CONH-), 1189 (C-O-C).

Functional Terminal. The products mentioned above as well as a certain amount of POSS or ethanol were dissolved in three-necked flask by anhydrous chloroform, stirred for 5 h at 80 °C, after precipitating in 10 volumes of n-hexane twice, the products were dried in vacuum at 45 °C for 24 h. The samples were washed two times with hexane to remove unreacted POSS. FTIR (cm^{-1}, KBr window): 2946-2867 ($-CH_2-CH_2-$), 17[illegible] (C=O), 1630-1534 (-CONH-), 1190 (C-O-C). ^1H NMR in $CDCl_3$ (ppm): δ5.252 (q, J=7.05 Hz, $-O-(CH_3)CH-CO-$), δ4.247 (t, J=4.86Hz, $-OCH_2CH_2O(C=O)-$), δ4.083 (t, J=6.68Hz, $-CH_2CH_2O(C=O)-$), δ3.668 (s, $-OCH_2CH_2-$), δ3.18 ($-CH_2NH-$), δ2.329 (t, J=7.51Hz, $-O(C=O)-CH_2CH_2-$), δ1.712-1.629 (m, $-O(C=O)-CH_2CH_2-$, $-CO-C(CH_3)H-O-$), δ1.442-1.364 (m, $-CH_2CH_2CH_2-$), δ0.97 (d, J=6.588 Hz, $-CH_3$(POSS)), δ0.62 (d, J=7.018 Hz, -CH- (POSS)).

Scheme 1 Synthesis of copolymers: Step (1), the synthesis of PEG-PCL by ROP; Step (2), synthesis of PEG-PCL-PLLA by ROP; Step (3), chain extension by HDI; Step (4), functional terminal.

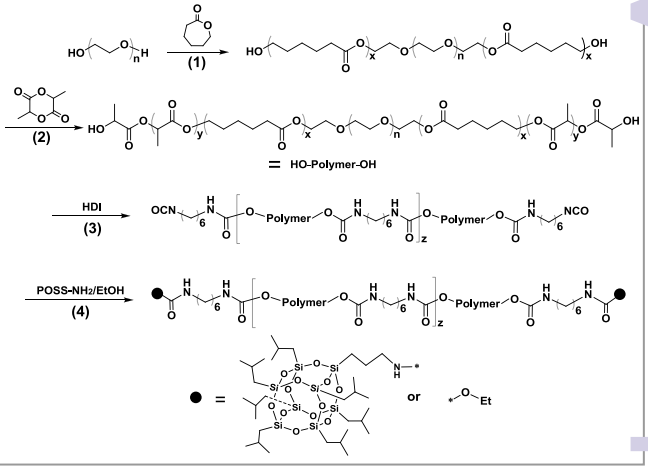

Sample Preparation. The obtained materials from synthesis and precipitation were cast from $CHCl_3$ solution, as indicated in the following example: the polymer (5 g) was dissolved in $CHCl_3$ (40 mL) and poured in a PTFE casting dish with the dimension of 10 cm × 10 cm, and then transferred to a chamber to allow for a slow solvent evaporation. Following 48 h, the films were put in a vacuum at 50 °C to remove any residual solvent. The resulting films were flexible and nearly 0.40 mm in thickness.

Characterization. ^{1}H NMR spectra were recorded in $CDCl_3$ at 400MHz in the AV400 (BRUKER) at 25 ^{o}C with deuterium solvents and TMS as an internal reference. Fourier transform infrared spectroscopy (FTIR) was recorded with Bruker Tensor-27 Fourier transform infrared spectrometer using the KBr disk method. Gel permeation chromatography (GPC) was performed on the system (Water 1515, Isocratic HPLC Pump and Water 2414 Refractive index Detector) to obtain the molecular weights and molecular weights distribution of the polymers at room temperature. Tetrahydrofuran was used as mobile phase with a flow rate of 1.0 mL/min with column temperature at 35 ^{o}C, and monodisperse polystyrene standard samples were used for calibration.

Differential scanning calorimetry (DSC) was performed using a DSC 200PC (NETZSCH) differential scanning calorimeter calibrated with indium. Glass transition temperature (Tg) and melting temperature (Tm) were measured according to the running conditions: the sample was heated from room temperature to 180 ^{o}C (Process I) or 100 ^{o}C (Process II) (first heating, 20 ^{o}C/min), kept isothermally for 5 min, cooled down to -100 ^{o}C, and heated again to 180 ^{o}C (second heating, 10 ^{o}C/min). Furthermore, the degree of crystallization for each block was calculated based on DSC according to the following equation:

$$\boldsymbol{\varphi_c^i} = \frac{|\Delta \boldsymbol{H_m}| - \Delta \boldsymbol{H_c}}{\boldsymbol{\omega_i} \Delta \boldsymbol{H_{m,0}}} \times \mathbf{100}\% \qquad (1)$$

where $\boldsymbol{\varphi_c^i}$ represented the degree of crystallinity of the component i, $\Delta \boldsymbol{H_m}$ and $\Delta \boldsymbol{H_c}$ were the measured enthalpies of melting and cold crystallization, respectively, $\Delta \boldsymbol{H_{m,0}}$ was the melting enthalpy for a 100% crystalline material and $\boldsymbol{\omega_i}$ was the fraction of the component i in the sample. The value taken for $\Delta \boldsymbol{H_{m,0}}$ of PLLA was 93 J/g, while for PCL was 148 J/g [22].

For optical microscopy observation, a Motic BA300 optical microscope equipped with a hot stage was used in this study.

The X-ray diffraction (XRD) data of the polymers were recorded with BRUKER D8 ADVANCE diffract meter using Cu Kα radiation from 5^o to 40^o at room temperature.

Uniaxial tensile tests were carried out at 25 ^{o}C with a crosshead speed of 50 mm/min. Samples measuring 20 mm×4 mm×0.4 mm were cut from the films obtained above using a fresh razor blade. The modulus of each sample was determined by linearly fitting the elastic portion of the stress-strain curve before the yielding point. Five dog bone-shaped samples were analyzed.

In vitro degradation of all samples was carried out as reported elsewhere [37]. Typically, preweighed samples were placed individually in test tubes containing phosphate buffered saline (PBS) at pH ~7.4. The films were removed from the buffer solution and cleaned for three 15 min cycles each with deionized water under sonication. Thereafter, the cleaned films were freeze dried for 24 h. Mass remaining (MR %) was calculated according to the following equation [38]:

$$\mathbf{MR}\ \% = \frac{\boldsymbol{m_r}}{\boldsymbol{m_i}} \times \mathbf{100}\% \qquad (2)$$

where $\boldsymbol{m_i}$ was initial mass, $\boldsymbol{m_r}$ was the remaining mass at different stages of incubation. The degradation study was conducted for a period of 2 months, with analysis of the mass remaining of the materials. Contact Angle was recorded by OCA20 (Data physics). The surface morphology was examined by scanning electron microscope (SEM, Hitachi S-4700).

MTT assay was used to test the cytotoxicity of the membranes. The 20 mm×30 mm samples were sterilized by washing with a 75% (v/v) ethanol solution in sterilized water, exposed to Co^{60} for 15 min, and then incubated in DMEM at a proportion of 3 cm^2/mL for 24 h at 37 ^{o}C to get the extract solution of the samples. The extract solutions were then filtered (0.22 μm pore size). L929 cells were resuspended in DMEM supplemented with 10% (v/v) Fetal Bovine Serum at a density of 1.0 ×10^4 cells/mL and 100 μL of cell resuspension solution was pipetted into 96-well micrometer plates. After incubated at 37 ^{o}C under 5% CO_2 atmosphere for 24 h, the medium was replaced by the previously prepared extracted dilutions (50 vol.%), with the culture medium as blank control and DMSO as negative control. After 24 h, 48 h, and 72 h of incubation, the morphologies of the cells in the plate were observed by using an inverted phase contrast microscope (Olympus IX50-S8F2). The cells were treated with 20 μL/well MTT (5 mg/mL in PBS solution) and incubated for another 4 h at 37 ^{o}C in a humidified atmosphere of 5 % of CO_2. Then the culture medium was removed and 200 μL/well of DMSO was added to dissolve the formed formazan crystals. After the plate was shaken for 15 min, the optical density (OD) was read on a multi-well microplate reader at 630 nm. The cytotoxicity

Table 1 Composition, GPC and contact angle data of the samples.

Sample	[a] $n_{,PEG}$	[a] $x_{,PCL}$	[a] $y_{,PLLA}$	[b] Mw	[b] PDI	T. F.	Contact Angle (^{o})
A	1	1.52	0.48	111350	1.530	EtO-	81.48(0.93)
B	1	1.37	1.19	84200	1.458	EtO-	87.86(2.45)
C	1	1.56	1.52	93780	1.483	EtO-	83.12(0.54)
D	1	1.56	1.52	97600	1.437	POSS-	103.49(2.67)
E	1	1.43	2.67	81330	1.414	EtO-	83.58(0.96)
F	1	0.93	1.13	99260	1.421	EtO-	77.86(3.21)

[a] Calculated from ^{1}H NMR. [b] Obtained by GPC. T. F. replaced terminal functional group.

for each membrane was tested by six averages of extract substrate. The relative growth rate (RGR %) was calculated according to the formula as below [39]:

$$\mathbf{RGR}\ \% = \frac{(OD)_{materials} - (OD)_{blank}}{(OD)_{negative\ control} - (OD)_{blank}} \times 100\% \qquad (3)$$

Blood compatibility was evaluated by Hemolysis %. Typically, Ethylenediaminetetraacetic acid (EDTA)-stabilized human blood samples were freshly obtained from healthy adult volunteers. First, 5 mL of blood sample was added to 10 mL of 0.9 % saline, and then red blood cells (RBCs) were isolated from serum by centrifugation at 2000 rap/min for 10 min. The RBCs were further washed 3 times with 10 mL of 0.9 % saline. The purified RBCs were then diluted to 50 mL 0.9 % saline. The PEG-PCL-PLLA-based membranes (10×10 mm^2 in area) were washed with distilled water 3 times and then put into a test tube with 9.8 mL 0.9 % saline and incubated for 30 min at 37 °C. After that, 0.2 mL of diluted blood was added into test tube and incubated for 2 hours at 37 °C. Similarly, 0.2 mL of diluted blood was added to 9.8 mL of distilled water and 0.9 % saline solution using as a positive and negative controls, respectively. After the incubation, all the samples were centrifuged at 2000 rap/min for 10 min. Then OD values were determined for the absorbance at 540 nm using a spectrophotometer (UV-2550, Japan). The hemolysis percentage (Hemolysis %) can be calculated by the following equation [40, 41]:

$$\mathbf{Hemolysis}\ \% = \frac{(OD)_{materials} - (OD)_{nc}}{(OD)_{pc} - (OD)_{nc}} \times 100\% \qquad (4)$$

where $(OD)_{materials}$ is the absorbance of the test samples; $(OD)_{pc}$ and $(OD)_{nc}$ are the absorbance of the positive and negative control, respectively. The hemolysis results were average of 6 measurements.

Results and Discussion

Synthesis of copolymer and structure characterization. To obtain multiblock copolymers consisting of PEG, PCL and PLLA units via urethane linkages, difunctional building blocks were required. For this purpose, double hydroxyl-terminated linear PEG-PCL-PLLA prepolymers with different molecular weight ratios were prepared. Firstly, PEG-PCL diols were synthesized; the structures were confirmed by the appearance of peak f at 4.24 ppm belonging to methylene protons of the PCL-CO-OC*H*$_2$-CH_2-O-PEG segment (Fig. 1(a)). PEG-PCL diols were further used as the macro-initiator to prepare PEG-PCL-PLLA prepolymers. The purified PEG-PCL-PLLA polymers were characterized by ^{1}H NMR (Fig. 1(b)). As shown in Fig. 1 (b), the peaks at 5.25 ppm and 4.38 ppm corresponded to the methane proton b and to the methane proton of lactide end group b' respectively. To analyze the crystalline properties systematically, calculated by ^{1}H NMR of the prepolymers, the relative proportion of PEG, PCL and PLLA blocks were obtained, as shown in Table 1.

Starting from the synthesized PEG-PCL-PLLA diols, a polycondensation using HDI was carried out. As shown in Fig. 1(c), the signal at 3.18 ppm was assigned to the methene groups conjoint to the -CONH- group [42], which confirmed the formation of urethane groups. Furthermore, the signal corresponding to the PLLA end groups (peak at 4.38 ppm) disappeared almost completely, also confirming that the condensation reaction proceeded correctly. Some other

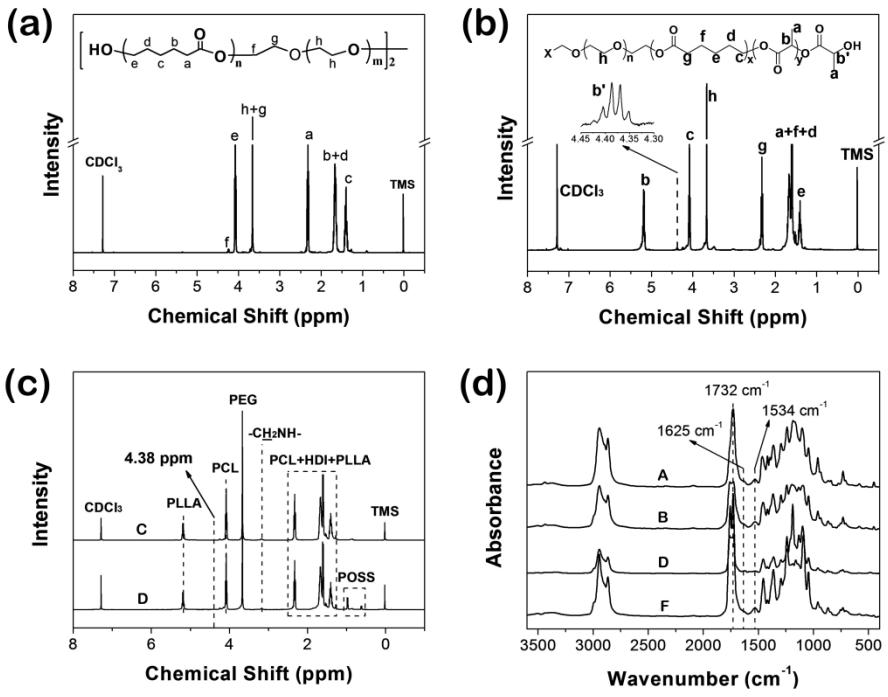

Fig. 1 ^{1}H NMR of (a) PEG-PCL; (b) PEG-PCL-PLLA; (c) the typical products, namely, sample C with ethoxy terminal group and D with POSS terminal; and (d) FTIR of selected samples.

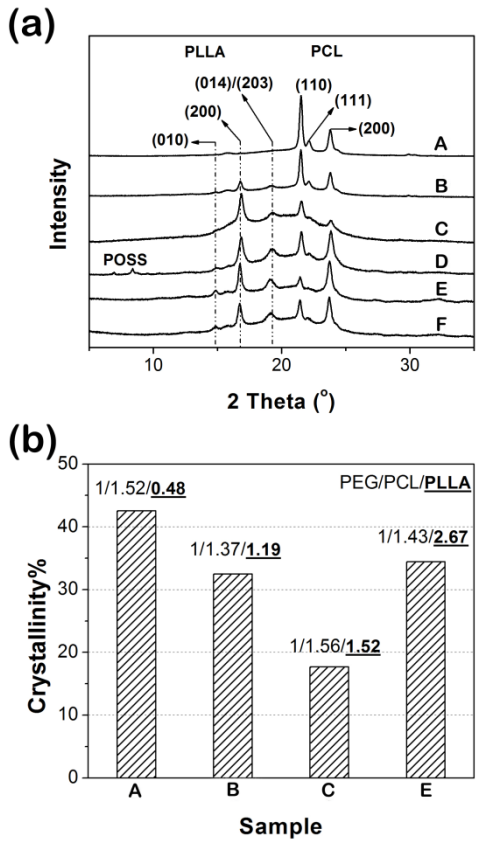

Fig. 2 (a) XRD of PEG-PCL-PLLA-based multi-block copolymers obtained by solution casting method, (b) degree of crystallinity of sample A, B, C and E, with PEG: PCL: PLLA composition value of 1:1.52:0.48, 1:1.37:1.19, 1:1.56:1.52 and 1:1.43:2.67, respectively.

characteristic peaks were marked in Fig. 1(c). In addition to ^{1}H NMR spectroscopy, FTIR measurements were conducted to confirm the molecular structure of the copolymers. The peak near 1732 cm^{-1} was the carbonyl group stretching from ester and amide groups, and peaks at 1625 cm^{-1} and 1534 cm^{-1} were attributed to amide I and amide II of amide groups in urethane. Additionally, the signals at 0.97 ppm of methyl and 0.62 ppm of methine in POSS (Fig. 1(c)) were assigned to the POSS terminal because sample D was washed two times with excessive hexane to remove any unreacted POSS.

In addition, Bismuth ethylhexanoate, an almost nontoxic chemical, could effectively catalyze the chain extension reaction [43], in conjunction with the mentioned four-step strategy to synthesize linear multi-copolymers with well-controlled chain lengths ratio, which provided a realistic possibility for industrialization.

Crystalline properties. It was well known that crystallinity played an important role in the degradation behavior. As it can be seen in XRD patterns, Fig. 2(a), all samples showed very sharp crystalline reflections at 2θ =21.4° and 23.6 °, corresponding to (110) and (200) lattice planes of PCL [26]. While, PLLA segments showed sharp crystalline reflections at 2θ =14.7 °, 16.6 ° and 19.0 °, corresponding to (010), (200) and the composite of (014) and (203) lattice planes [44]. However, the

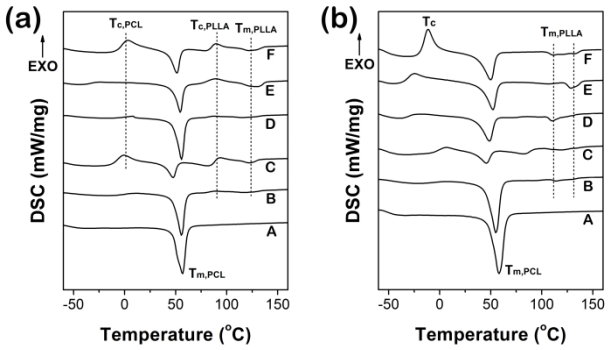

Fig. 3 DSC curves of PEG-PCL-PLLA multi-block copolymers with different thermal treatment: (a) heating to 180 °C and then quenched (Process I), (b) heating to 100 °C and then quenched (Process II).

PEG segments were amorphous and there was no PEG crystalline reflection in sample A based on XRD. The crystallinity of the sample of A, B, C, D, E and F was calculated to be approximately 42.55%, 28.23%, 17.68%, 32.49%, 34.42% and 21.55%, respectively, from the XRD by using JADE.

Analyzing sample A, B and E, we found that PLLA crystallization ability was enhanced obviously with the increase of PLLA content, which can be affirmed by the increase in the intensity of (200) crystal plane (Fig. 2 (a)). On the contrary, (110) crystal plane intensity of PCL was significantly reduced, indicating that crystallization ability of PCL was weakened. It was because PLLA disrupted the crystallization of PCL, resulting in imperfect crystal structures and subsequently decreasing in melting temperature and crystallinity. When PCL was the main components, the crystallization of PLLA was interfered, directly resulting in no diffraction peak in XRD and melting peak in DSC curve for sample A, so PLLA in the sample A was almost amorphous. Thus we concluded that only when PLLA content reached a certain extent, can PCL and PLLA crystal coexist in the copolymer matrixes. When the content of PLLA was further increased, the chemical regularity of the copolymer matrix was further damaged, which gave rise to the crystallinity decreasing (sample B). When the PCL and PLLA components were with similar proportion, its chemical regularity reached the minimum, endowing the lowest degree of crystallinity for sample C. As to sample D, even in the similar component as sample C, the introduction of POSS with strong interaction, which may play the role of molecular nucleation agents, was conducive to the crystallization of polymers, especially to the PCL blocks, resulting in the crystallinity increasing remarkably. Namely, sample D was with extremely higher crystallinity than sample C. As it can be seen from Fig. 2(a), the relative intensity of PCL crystal plane (200) in sample D increased significantly comparing to sample C, which also indicated that the POSS played a role in inducing crystallization. In addition, sample D with POSS-terminal showed significant POSS crystallization peak, as marked in Fig. 2(a), which indicated that POSS in the sample formed crystalline aggregates.

Table 2 Thermal properties and degree of crystallinity of PEG-PCL-PLLA multiblock copolymers obtained from DSC by Process I.

Samples	T_g (°C)	$T_{c,PCL}$ (°C)	$\Delta H_{c,PCL}$ (J/g)	$T_{m,PCL}$(°C)		$\Delta H_{m,PCL}$ (J/g)	$T_{c,PLLA}$ (°C)	$\Delta H_{c,PLLA}$ (J/g)	$T_{m,PLLA}$ (°C)	$\Delta H_{m,PLLA}$ (J/g)	$\varphi_{c,PCL}$%	$\varphi_{c,PLLA}$%
				Onset	Peak							
A	-53.4	-	-	47.3	56.7	-65.82	-	-	-	-	64.64	-
B	-60.1	-	-	47.8	55.7	-42.31	87.7	1.29	118.6	-2.91	52.32	5.81
C	-54.8	-2.0	11.24	39.4	47.4	-20.12	91.3	4.46	122.3	-4.90	11.18	1.43
D	-50.3	-	-	48.4	55.6	-52.12	86.1	1.28	116.9	-3.81	65.60	8.23
E	-55.0	-26.2	2.41	47.4	54.5	-35.52	88.8	5.58	129.5	-11.78	54.79	13.84
F	-54.3	2.7	22.49	43.5	51.2	-30.4	88.7	7.33	122.2	-8.12	11.66	2.42

As shown in Fig. 2(b), with the increase of the PLLA content, the degree of crystallinity in total reduced firstly and increased later. When PLLA content increased to the value of sample E, PLLA itself formed a good crystallinity, which contributed to recovery of degree of crystallinity.

Competitive crystallization of the multi-block copolymers. Melting properties of the copolymers were determined by DSC as shown in Fig. 3. The endothermic peaks at temperature close to 50 °C corresponded to the melting of PCL, while those of higher temperature (about 125 °C) corresponded to the melting of PLLA. We observed that PLLA regions exhibited multiple melting peaks except for sample A (Fig. 3(b)), which can be attributed to the presence of crystals with different size [26]. It was evident that the T_m as well as the enthalpies of melting was strongly influenced by the composition of the copolymer. As shown in Fig. 3(a), when the first heating temperature reached 180 °C (Process I), polymer segments were all in melting state. During the quench process, the slow crystallization of PLLA resulted in the presence of PLLA imperfect crystals. Accordingly, the cold crystallization of PLLA (~90 °C) emerged (except for sample A) in the second heating. PCL can exhibit better crystallinity than PLLA, which was due to relative fast crystallization rate of PCL. However, both sample C and F showed dual cold crystallization. It was mostly attributed to uncompleted crystal of PCL and PLLA because the mole ratio of PCL and PLLA equaling to 1:1, which resulted in low chemical regularity of whole chains.

When the first heating temperature reached 100 °C (Process II), as shown in Fig. 3 (b), only PCL segments were in melting state, and the PLLA segments were annealing which ensured the PLLA crystallize completely. Therefore, there was no obvious cold crystallization of PLLA during second heating. Furthermore, the crystallization of PLLA had occurred sufficiently in the situation, which resulted in the values of PLLA crystallinity being generally higher than that obtained from Process I except for sample D, as shown in Fig. 4 (a).

The results showed that, when PLLA was with high crystallinity (Process II), crystallinity of PCL in all samples except for sample D were lower than that obtained from

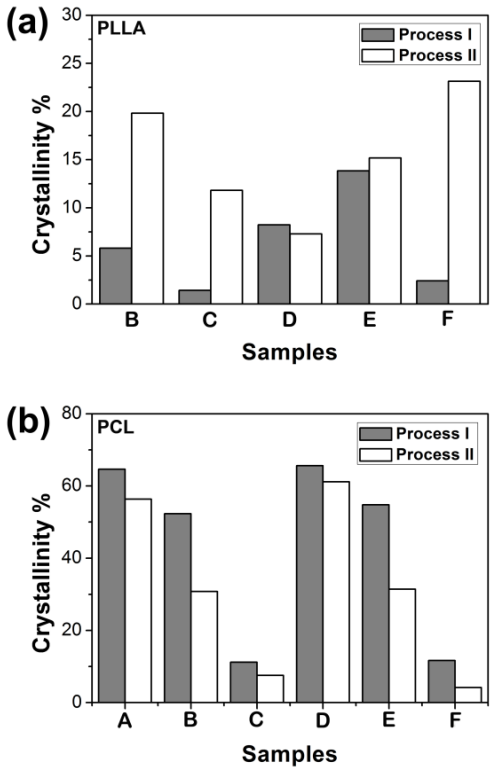

Fig. 4 Crystallinity of (a) PLLA and (b) PCL segments with different thermal treatment: process I, heating to 180 °C and then quenched; process II, heating to 100 °C and then quenched.

Process I, as shown in Fig. 4 (b). This indicated that during th heat treatment, the crystallization ability of the components was in a competition state, which was termed "competitive crystallization". Clearly, PCL and PLLA each can form individu crystalline microstructure due to the different unit ce parameters as well as crystal conformation, giving rise t microphase separation driven by thermodynam incompatibility; in addition, the PCL and PLLA (even POSS fo sample D) were in one molecular chain. Therefore, hi h

Table 3 Thermal properties and degree of crystallinity of PEG-PCL-PLLA multiblock copolymers obtained from DSC by Process II.

Samples	T_g(°C) Mid.	$T_{c,peak}$ (°C)	ΔH_c (J/g)	$T_{m,PCL}$(°C) Onset	$T_{m,PCL}$(°C) Peak	$\Delta H_{m,PCL}$ (J/g)	$T_{m,PLLA}$(°C)	$\Delta H_{m,PLLA}$ (J/g)	$\varphi_{c,PCL}$%	$\varphi_{c,PLLA}$%
A	-50.8	-	-	49.2	58.1	-57.4	-	-	56.37	-
B	-54.8	-	-	37.1	48.8	-24.9	110.2	-5.53	30.79	19.83
C	-52.0	5.6	6.29	35.9	45.6	-12.3	120.1	-3.63	7.56	11.82
D	-51.2	-	-	45.8	54.9	-48.6	114.1	-2.24	61.17	7.29
E	-54.7	-25.9	9.11	41.7	52.1	-28.1	107.0,129.3	-1.214,-5.584	31.42	15.18
F	-51.4	-11.6	26.68	38.4	50.0	-29.5	112.3~131.7	-7.569	4.16	23.15

crystallinity of one component will significantly restrict the crystallization ability of another component. For typical example, the complete PLLA crystallization of sample F (Process II) resulted in a greater degree of inhibition of PCL crystallization, which can be affirmed by the PCL cold crystallization in Fig. 3(b) being stronger than that in Fig. 3(a).

The crystallization of sample D was different with other samples. On the one hand, appropriate amount of POSS aggregation may induce the crystallization of PCL and PLLA by acting as nucleation agents. Thus, in the Process I, we observed that under the same PCL and PLLA components and heat treatments, the crystallinity of both PCL and PLLA in sample D was significantly higher than that in sample C (Fig. 4).

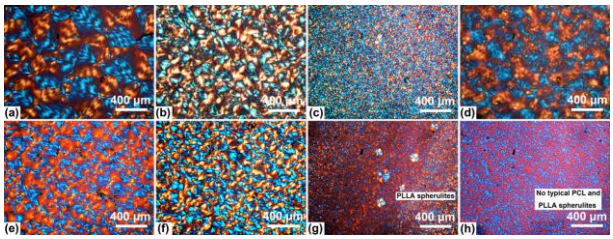

Fig. 5 Polarizing optical micrographs of the multi-block copolymers: (a), (b), (c) and (d) representing sample A, B, C and D, respectively, which were prepared by heating the samples to 180°C and crystallizing isothermally at 40 °C for 2h; (e), (f), (g) and (h) representing sample A, B, C and D, respectively, which were prepared by heating the samples to 180°C, moving directly to another hot plate at 100°C, and then crystallizing isothermally at 40 °C for 2h.

On the other hand, the terminal POSS with strong interaction will restrict the thermal movement so as to crystallization of the whole molecular chain. Accordingly, both PLLA (Fig. 4(a)) and PCL (Fig. 4(b)) in sample D showed lower crystallinity than that obtained in Process I because of restriction of POSS aggregates on the ordered arrangement of PLLA and PCL segments under the heat treatment in Process II. The data based on DSC were all listed in Table 2 and Table 3.

Fig. 5 presented polarizing optical micrographs of the multi-block copolymers, which were prepared by different heat treatment. As it can be seen, sample A showed good spherulitic morphology in Fig. 5, which was due to the highest chemical regularity. The typical PCL spherulites were marked in Fig. 5(a) and Fig. 5(b). With the increase of PLLA content, the chemical regularity decreased, thus samples B, C and D al

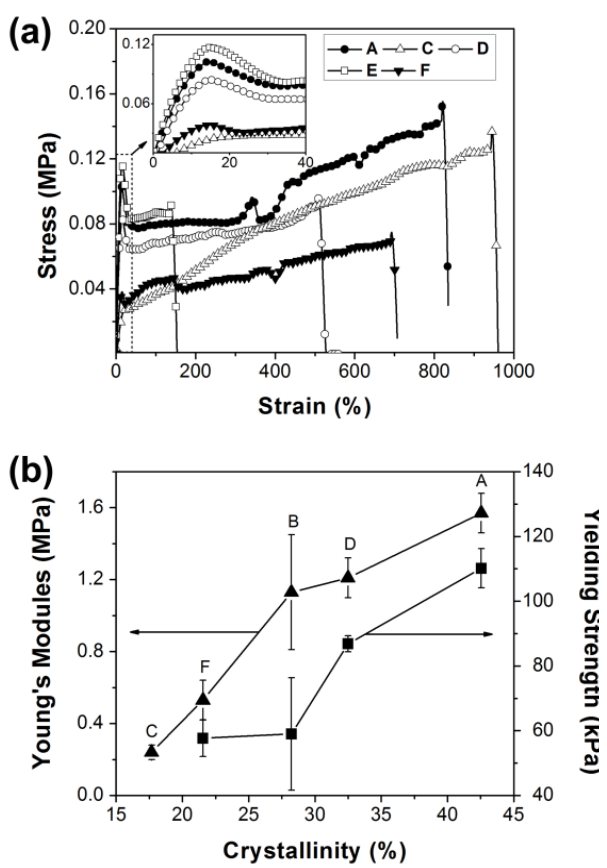

Fig. 6 (a) Stress-Strain curve of selected samples, (b) curves of Young's modules and yielding strength vs. crystallinity.

Table 4 Mechanical properties of PEG-PCL-PLLA-based multiblock materials.

Samples	Yielding Strength (kPa)	Stress Strength (kPa)	Young's Modules (MPa)	Elongation (%)
A	110.17(6.09)	141.29(7.71)	1.57(0.11)	746.04(96.55)
B	59.03(17.39)	37.99(14.56)	1.13(0.32)	783.57(46.73)
C	-	139.63(13.90)	0.24(0.04)	944.05(53.02)
D	86.84(2.45)	82.37(8.96)	1.21(0.11)	446.09(74.40)
E	104.76(9.36)	78.96(10.26)	1.61(0.17)	124.68(35.54)
F	57.39(5.68)	76.51(17.06)	0.53(0.11)	598.47(81.57)

showed smaller spherulites than that of sample A. Furthermore, as discussed above, the crystallinity of PLLA treated in Process I was lower than that treated in Process II due to the high cooling rate as well as slow crystallization rate of PLLA. Therefore, no obvious PLLA spherulites were observed in Fig. 5(c). However, during the Process II, sample C had enough annealing time, giving rise to significant PLLA spherulites (Fig. 5(g)). In addition, because of the competitive crystallization between PCL and PLLA segments in one chain, the sufficient crystallization of PLLA will restrict crystallization of PCL more, which leaded to smaller spherulites in Fig. 5(e) to Fig. 5(h) comparing to that in Fig. 5(a) to Fig. 5(d), respectively. Also according to DSC analysis, in Process I, POSS in sample D induced crystallization of the PCL and PLLA significantly, so sample D presented typical spherulite morphology (Fig. 5(d)); while during Process II, the behavior of the terminal POSS restricted crystallization of PCL and PLLA segments and then restrict formation of typical spherulites of copolymer in Fig. 5(h).

Therefore, we concluded that depending on the composition and different heat treatments, samples attained different degree of crystallinity, so as to realize the effective control of mechanical and degradation properties.

Stress-Strain Curve. The mechanical data were listed in Table 4 and stress-strain curves of the selected samples were shown in Fig. 6(a). The copolymers showed different crystalline characteristics as discussed above, which endowed the tunable mechanical properties, such as Young's Modules and yielding strength. As shown in Fig. 6(b), for samples A, B, C, D and F, both Young's Modules and yielding strength increased with the increasing of crystallinity. However, when PLLA content reached as sample E, the intrinsic properties of crystalline PLLA would contribute to the mechanical properties, eventually accounting for the largest elastic modulus and relative high yielding strength (Fig. 6(a) inset and Table 4). Also for sample E, the elongation at break decreased to 124.68%, which was far less than the application requirements of blood vessel substitute. In addition, there was no remarkable yielding in sample C with lowest modulus (Fig. 6(a)), because it was with the lowest crystallinity. Finally, it was worth noting that the POSS can induce crystallization in the situation and act as mechanical enhancement agent accordingly, which resulted in sample D being with much higher elastic modulus than that of sample C (Table 4) and maintaining a high elongation at break.

Bio-degradation testing. The controllable degradation rate was useful for various biomedical applications [45] because it will directly influence the in vivo performance of a scaffold. Changes in composition can vastly change the degradation behavior [33]. So it was expected that different weight ratios of PEG, PCL and PLLA in the copolymer might contribute to tunable degradation rates. Consequently, we investigated the effect of composition on the degradation profile of the copolymers by incubating samples in PBS buffer at 37 ^{o}C over the course of 2 months.

As known, polyesters presented surface or bulk degradation mechanisms depending on the two stages, which was water diffusion and hydrolysis of ester bonds. At the early stage, degradation took place mainly in the surface, so contact angel was necessary to evaluate the surface hydrophilicity. The

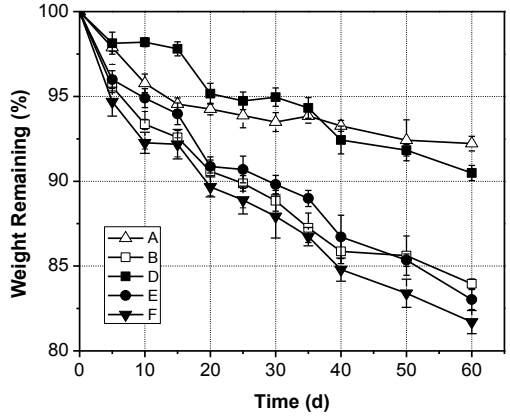

Fig. 7 Mass Loss profiles of selected samples during 2 months in vitro degradation. The thickness of all selected samples was about 0.4mm.

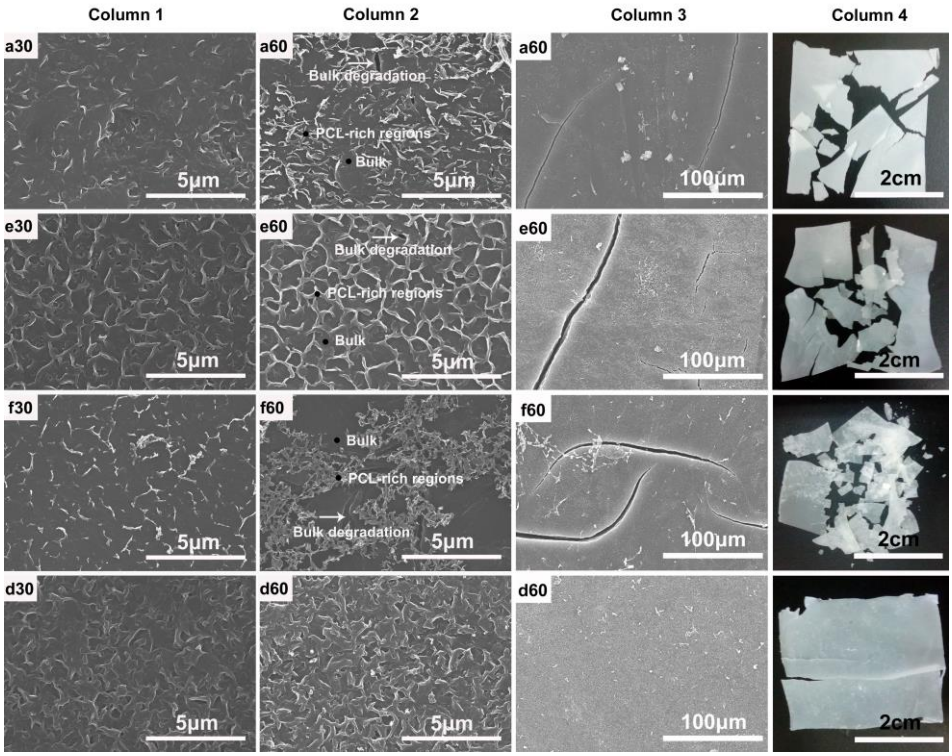

Fig. 8 Surface morphologies of selected samples after degradation for 30 days (a30 for sample A, e30 for sample E, f30 for sample F and d30 for sample D, column 1) and 60 days (a60 for sample A, e60 for sample E, f60 for sample F and d60 for sample D, column 2 and 3) obtained by SEM and the images of mentioned samples after bio-degradation for 60 days (column 4).

contact angle for all samples was between 77.86° to 103.49° and listed in Table 1. The key parameters in the bio-degradation process were crystallinity, hydrophilicity and the content of PLLA in the study.

As observed, the high content of PLLA, low crystallinity and high hydrophilicity all accelerated bio-degradation rate. For examples, comparing sample A with sample E (Fig. 7), which were with same PEG-PCL contents, degradation rate of the materials increased significantly with PLLA increasing. Sample B degraded with a rapid rate from the beginning, because it was with low crystallinity; while sample E was with higher crystallinity and giving rise to lower degradation rate accordingly. This was due to the crystalline regions showed the tendency to retard water uptake. Additionally, sample D was with slow degradation rate in 35 days, which could be attributed to the high crystallinity of PCL and the strong hydrophobic effect POSS, giving rise to the highest contact angle with 103.49°. However after 35 days the degradation occurred significantly, herein PLLA ingredient became the dominant factor, resulting in sample D with a faster degradation rate than that of sample A. As to sample F, with the lower PCL as well as highest PEG content, showed the fastest rate of degradation in all mentioned samples. It can be mainly attributed to the increasing of hydrophilicity, namely, with the lowest contact angle of 77.86°, which was conductive to water uptake.

Furthermore, the surface morphologies of selected samples were obtained by SEM. As shown in Fig. 8, the roughness of the material surface increased significantly with the occurrence of degradation, which was caused by surface degradation and dissolution. Because the PLLA degraded with a faster rate than that of PCL, the bulges in the surface were considered to be PCL-rich regions, as marked in Figure 8-a60, e60 and f60 (column 2). The bulk degradation caused the pores (as marked by arrows, column 2) and the cracks (column 3) in the materials, and the crack diffusion eventually resulted in the damage of the material. According to the images in Figure 8 (column 4), sample A, E and F showed a significant

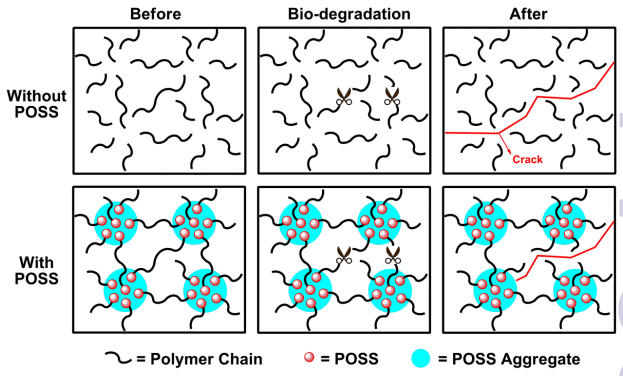

Fig. 9 Proposed mechanism of the POSS protection effect on the integrity of materials after degradation.

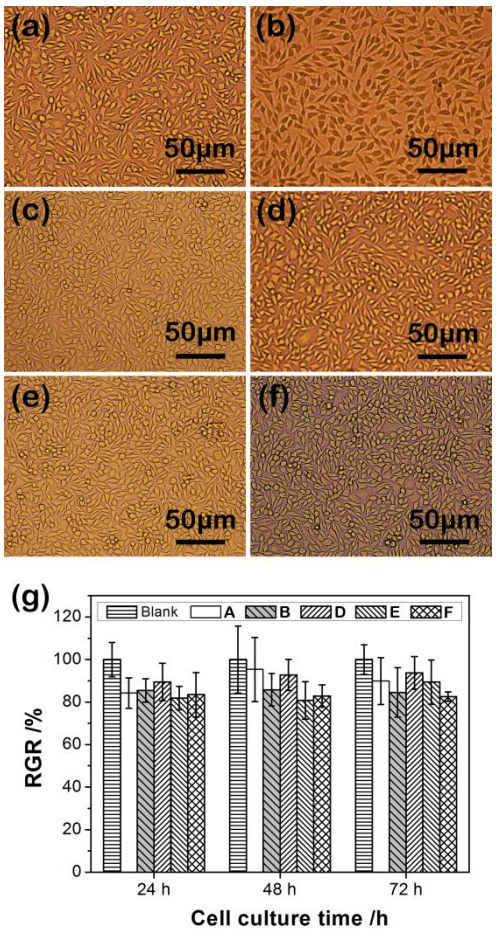

Fig. 10 Photomicrographs of the L929 cells incubated for 72h in the negative control and the extract substrates of samples composites (a-f). (a for Blank; b for Sample A; c for Sample B; d for Sample D; e for Sample E and f for Sample F), (g) Relative growth rate (RGR%) of L929 cells cultured for 24 h, 48 h and 72 h on samples compared with that on control substrate.

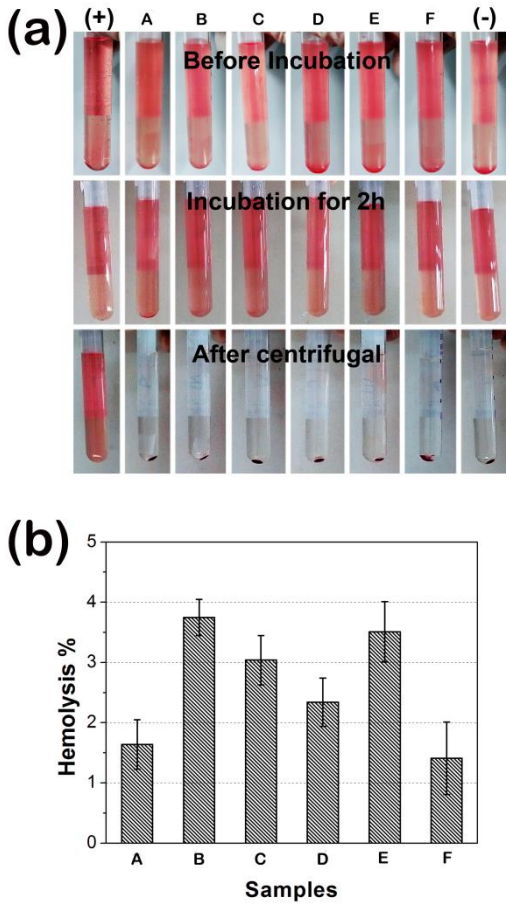

Fig. 11 (a) Photograph of hemolysis experiment procedure, (b) Hemolysis % of PEG-PCL-PLLA-based membranes.

degradation. However, the existence of POSS made sample D exhibit a good step-degradation, namely, the high hydrophobicity of POSS ensure the sample be with a slow degradation rate in the early stage and degraded quickly in the second stage, which can effectively reduce the possibility of thrombosis when it was used for blood treatments. In addition, proposed mechanism of the POSS protection effect was shown in Fig. 9. Concretely, POSS formed aggregates due to the strong interaction, which can act as physical cross-linking points. Under the similar degradation situation, the cross-linking points restricted crack transfer, and connected a plurality of micro-structure unit, ensuring the integrity of sample D after degradation.

Thus, we can design the materials with suitable PEG, PCL and PLLA contents to make sure the materials exhibited a controllable degradation rate. In addition, we can introduce POSS to achieve a slow degradation rate in the early stage, and maintain the integrity of the material in a long period. According to the controlled degradation of the project as well as good biocompatibility design principles, we combined the advantages of PEG, PCL, PLLA, and the POSS to prepare PEG-PCL-PLLA-POSS hybrid polymer of biological material having a novel structure and composition. Conveniently, we could achieve different proportions precisely through block copolymerization and "precursor-chain extension" method mentioned in this study.

Cytotoxicity. MTT assay was used to test the cytotoxicity of the membranes. As indicated in Fig. 10, the morphologies of L929 cells incubated for 72 h in the extract substrates of the membranes all showed spindle, triangular, and quadrangular shapes with good growing conditions. The viability of L929 cells cultured in the extract substrates of the membranes had no significant difference with that in the cell culture medium, reflecting that the membranes showed no cytotoxicity. RGR% of sample with POSS termination was highest, which indicate POSS molecules improved the cytotoxicity of materials to some extent. We can find all the RGR % values of the cells cultured on the composite substrates for 3 days were all above 80.77%, which indicated the materials showed no toxicity on the cell viability.

Blood-compatibility. The hemolysis ratio was widely used to evaluate the destructive degree of any implant material t

erythrocytes [46]. As shown in Fig. 11, the Hemolysis % of the samples was all in 1.41% to 3.75% range, which indicated that the materials were all acceptable for clinical application (being less than 5%). It was worth emphasized that the introduction of POSS slightly improved the blood compatibility. In addition, the increasing of PEG content (sample F) was also conductive to the blood compatibility which was probably due to the improvement of hydrophilicity.

Conclusions

In order to obtain a materials with suitable bio-degradation performance and good biocompatibility, PEG-PCL-PLLA-based poly (ester-urethane) s with different segment ratios were successfully fabricated, which showed good cytocompatibility, and blood-compatibility, namely, with RGR % more than 80.77 % as well as Hemolysis % lower than 3.75 %. Moreover, the crystallization, mechanical behaviour and degradation rate could be effectively modulated by adjusting the terminal functional groups and the segment length of PEG, PCL and PLLA in the synthesis of PEG-PCL-PLLA diol precursor. It was worth noting that the POSS not only acted as crystallization reduce agent and enhanced the mechanical properties accordingly, but also ensured good step degradation of materials. The tunable mechanical behaviour, good cytocompatibility and blood-compatibility, in conjunction with the controllable degradation rate, classified these bio-materials for numerous biomedical applications.

Acknowledgements

The authors thank the National Natural Science Foundation of China (No. 51273017), Polymer Chemistry and Physics, Beijing Municipal Education Commission (BMEC, No. XK100100640) for financial support.

Notes and references

1 M. M. Kose, S. Onbulak, I. I. Yilmaz and A. Sanyal, *Macromolecules* 2011, **44** (8), 2707-2714.
2 R. Wang, W. Chen, F. Meng, R. Cheng, C. Deng, J. Feijen, and Z. Zhong, *Macromolecules* 2011, **44** (15), 6009-6016.
3 T. Chung-Kan, K. Chao-Yin, Y. Shu-Rui, Y. Chin-Yu, M. B. Eric, H. Simon, C. I-Ming and C. Ming-Huei, *Biomaterials* 2014, **35**, 1163-1175.
4 P. Y. Ni, Q. X. Ding, M. Fan, J. F. Liao, Z. Y. Qian, J. C. Luo, X. Q. Li, F. Luo, Z. M. Yang and Y. Q. Wei, *Biomaterials* 2014, **35**, 236-248.
5 H. X. Dan, V. Cédryck, A. G. Fisher, S. M. Hamlet, Y. Xiao, D. W. Hutmacher and S. Ivanovski, *Biomaterials* 2014, **35**, 113-122.
6 R. Zheng, H. C. Duan, J. X. Xue, Y. Liu, B. Feng, S. F. Zhao, Y. Q. Zhu, Y. Liu, A. J. He, W. J. Zhang, W. Liu, Y. L. Cao and G. D. Zhou, *Biomaterials* 2014, **35**, 152-164.
7 A. J. Melchiorri, N. Hibino, T. Yi, Y. U. Lee, T. Sugiura, S.Tara, T. Shinoka, C. Breuer and J. P. Fisher, *Biomacromolecules* 2015, **16** (2), 437-446.
8 C. Huang, S. Wang, L. Qiu, Q. Ke, W. Zhai and X. Mo, *ACS Appl. Mater. Interfaces* 2013, **5**, (6), 2220-2226.
9 J. Guan and W. R. Wagner, *Biomacromolecules* 2005, **6** (5), 2833-2842.
10 Y. Zhu, C. Gao, X. Liu and J. Shen, *Biomacromolecules* 2002, **3** (6), 1312-1319.
11 H. Seyednejad, W. Ji, F. Yang, C. F. van Nostrum, T. Vermonden, J. J. J. P. van den Beucken, W. J. A. Dhert, W. E. Hennink and J. A. Jansen, *Biomacromolecules* 2012, **13** (11), 3650-3660.
12 S. Lee, S. Cho, M. Kim, G. Jin, U. Jeong and J. Jang, *ACS Appl. Mater. Interfaces* 2014, **6**, 1082-1091.
13 B. A. Allo, S. G. Lin, K. Mequanint and A. S. Rizkalla, *ACS Appl. Mater. Interfaces* 2013, **5**, 7574-7583.
14 P. Dinarvand, E. Seyedjafari, A. Shafiee, A. B. Jandaghi, A. Doostmohammadi, M. H. Fathi, S. Farhadian and M. Soleimani, *ACS Appl. Mater. Interfaces* 2011, **3**, 4518-4524.
15 M. Nelson, R. Diana, M. Albino, F. Susana, A. F. Nuno, N. M. Joao, L. R. Rui and M. N. Nuno, *ACS Nano* 2014, **8** (8), 8082-8094.
16 Y. B. Kim and G. H. Kim, *ACS Comb. Sci.* 2015, **17**, 87-99.
17 Q. C. Zhang, K. Tan, Y. Zhang, Z. Y. Ye, W. S. Tan and M. Lang, *Biomacromolecules* 2014, **15**, 84-94.
18 J. Lv, L. Chen, Y. Zhu, L. Hou and Y. Liu, *ACS Appl. Mate Interfaces* 2014, **6** (7), 4954-4964.
19 J. Qiu, J. Li, G. Wang, L. Zheng, N. Ren, H. Liu, W. Tang, H Jiang and Y. Wang, *ACS Appl. Mater. Interfaces* 2012, **5**(2), 344-350.
20 F. K. Kasper, K. Tanahashi, J. P. Fisher and A. G. Mikos, *Nat. protoc.* 2009, **4** (4), 518-525.
21 R. G. Pauck and B. D. Reddy, *Med. Eng. Phys.* 2015, **37** (1), 1 12.
22 Z. B. Ning, N. Jiang and Z. H. Gan, *Polym. Degrad. Stab.* 2014, **107**, 120-128.
23 I. Navarro-Baena, J. M. Kenny and L. Peponi, *Polym. Degrad. Stab.* 2014, **108**, 140-150
24 I. Navarro-Baena, A. Marcos-Fernández, A. Fernández-Torres, J. M. Kenny and L. Peponi, *RSC Adv.* 2014, **4**, 8510-8524.
25 X. Deng, S. Zhou, X. Li, J. Zhao and M. Yuan, *J. Control Release* 2001, **71** (2), 165-173.
26 B. Alvarado-Tenorio, A. Romo-Uribe and P. T. Mather, *Macromolecules* 2011, **44** (14), 5682-5692.
27 K. Wu, M. Huang, K. Yue, C. Liu, Z. Lin, H. Liu, W. Zhang, C. Hsu, A. Shi, W. Zhang and S. Z. D. Cheng, *Macromolecules* 2014, **47** (14), 4622-4633.
28 W. Zhang, Y. Li, X. Li, X. Dong, X. Yu, C. Wang, C. Wesdemiotis, R. P. Quirk and S. Z. D. Cheng, *Macromolecules* 2011, **44** (8), 2589-2596.
29 W. Wang, Y. Guo and J. U. Otaigbe, *Polymer* 2009, **50** (24), 5749-5757.
30 P. T. Knight, K. M. Lee, H. Qin and P. T. Mather, *Biomacromolecules* 2008, **9** (9), 2458-2467.
31 Q. Guo, P. T. Knight, J. Wu, P. T. Mather, *Macromolecules* 2010, **43** (11), 4991-4999.
32 X. Gu, J. Wu and P. T. Mather, *Biomacromolecules* 2011, **12** (8), 3066-3077.
33 P. T. Knight, K. M. Lee, T. Chung and P. T. Mather, *Macromolecules* 2009, **42** (17), 6596-6605.
34 L. Wang, S. Di, W. Wang, H. Chen, X. Yang, T. Gong and S. Zhou, *Macromolecules* 2014, **47** (5), 1828-1836.
35 M. Zhang, H. Liu, W. Shao, K. Miao and Y. Zhao, *Macromolecules* 2013, **46** (4), 1325-1336.
36 E. A. Jackson, Y. Lee and M. A. Hillmyer, *Macromolecules* 2013, **46** (4), 1484-1491.
37 J. Xue, M. He, H. Liu, Y. Niu, A. Crawford, P. D. Coates, D. Chen, R. Shi and L. Zhang, *Biomaterials* 2014, **35** (34), 9395-9405.
38 T. Wu, M. Frydrych, K. O Kelly and B. Chen, *Biomacromolecules* 2014, **15** (7), 2663-2671.

39 W. Guo, H. Kang, Y. Chen, B. Guo and L. Zhang, *ACS Appl. Mater. Interfaces* 2012, **4** (8), 4006-4014.
40 Z. X. Meng, W. Zheng, L. Li and Y. F. Zheng, *Mater. Sci. Eng.* C 2010, **30** (7), 1014-1021.
41 H. Wang, Y. Feng, Z. Fang, W. Yuan and M. Khan, *Mater. Sci. Eng. C* 2012, **32** (8), 2306-2315.
42 L. Wang, X. Jing, H. Cheng, X. Hu, L. Yang and Y. Huang, *Ind. Eng. Chem. Res.* 2012, **51** (33), 10731-10741.
43 B. Xu, L. Li, K. Zhang, P. M. Macdonald, M. A. Winnik, R. Jenkins, D. Bassett, D. Wolf and O. Nuyken, *Langmuir* 1997, **13** (26), 6896-6902.
44 T. Isono, Y. Kondo, I. Otsuka, Y. Nishiyama, R. Borsali, T. Kakuchi and T. Satoh, *Macromolecules* 2013, **46** (21), 8509-8518.
45 C. Yang, H. Wu, J. Sun, H. Hsiao and T. Wang, *ACS Appl. Mater. Interfaces* 2013, **5** (21), 10985-10994.
46 J. Wang, Y. He, M. F. Maitz, B. Collins, K. Xiong, L. Guo, Y. Yun, G. Wan and N. Huang, *Acta Biomaterialia* 2013, **9** (10), 8678-8689.